Heliyon 9 (2023) e17280

Contents lists available at ScienceDirect

Heliyon

journal homepage: www.cell.com/heliyon

Structural, harmonic force field and vibrational studies of cholinesterase inhibitor tacrine used for treatment of Alzheimer's disease

Tom Sundius [a], Silvia Antonia Brandán [b,*]

[a] Department of Physics, University of Helsinki, Finland
[b] Cátedra de Química General, Instituto de Química Inorgánica, Facultad de Bioquímica. Química y Farmacia, Universidad Nacional de Tucumán, Ayacucho 471, 4000, San Miguel de Tucumán, Tucumán, Argentina

ARTICLE INFO

Keywords:
Tacrine
Molecular structure
Harmonic force fields
Vibrational analysis
DFT calculations

ABSTRACT

Different structures of free base (FB), two cationic forms (CA) and three hydrochloride forms (HCl) of cholinesterase inhibitor tacrine used for treatment of Alzheimer 's disease was evaluated using hybrid B3LYP calculations in order to perform their complete vibrational assignments using the scaled harmonic force fields. Structures of anhydrous form of tacrine have been optimized in gas phase and in aqueous solution. The structure of form III HCl is in agreement with the experimental determined by X-ray diffraction while the predicted IR, Raman, ^{1}H– ^{13}C NMR and UV spectra show good correlations with the corresponding experimental ones. Energy values show that the three forms of HCl can exist in both media because these energetic values decrease from 35.15 kJ/mol in gas phase to 5.51 kJ/mol in solution. For the most stable species of tacrine, the following stability order using natural bond orbital (NBO) studies was found: form I HCl > form III HCl > form I CA > FB. CA presents the higher solvation energy value, as reported for hydrochloride species of alkaloids and antihypertensive agents. The structural parameters of form III of HCl present better concordance and corresponds to that experimental observed in the solid phase. Higher topological properties of form III together with the strong N2–H26···Cl31 interaction could justify the presence of this form in the solid phase and in solution and the higher stabilities in both media. The gap values support the higher reactivity of form III while FB is the less reactive species in both media. Complete vibrational assignments for FB, CA and HCl species together with the corresponding scaled force constants are reported.

1. Introduction

In this work, different cationic and hydrochloride structures derived from anhydrous tacrine, an aminoacridine derivative with cognitive stimulating property were studied together with the free base to perform the assignments of vibrational spectra because so far, the complete assignments were not reported yet. From 1950, tacrine was used experimentally to treat reverse cholinergic coma in animals and, since 1993 its use was approved by the US Food and Drug Administration to treat Alzheimer's disease [1,2]. Thus, the interest in studying it has considerably increased, as it is evidenced by multiple studies carried out from different points of view [3–16]. Sorrenti et al. have established the presence of a unique anhydrous crystalline phase of tacrine hydrochloride using the

* Corresponding author.
E-mail addresses: tom.sundius@helsinki.fi (T. Sundius), silvia.brandan@fbqf.unt.edu.ar (S.A. Brandán).

https://doi.org/10.1016/j.heliyon.2023.e17280
Received 14 August 2022; Received in revised form 12 June 2023; Accepted 13 June 2023
Available online 19 June 2023

recrystallization of hot saturated solutions of two mono and di-hydrate forms obtained from different solvents [17]. Those studies have evidenced two forms of tacrine by using IR spectra and physicochemical properties but in that work, their structures are not reported. In many studies on complexes of Human carboxylesterase 1 with huprine and/or tacrine as free base were also reported [18,19] while in other works on synthesis of new tacrine derivatives only the biological activities are evaluated but not the structures of these new derivatives [20–22]. However, Moris et al. have determined an experimental orthorhombic pseudo polymorph structure of tacrine hydrochloride by using X-ray diffraction from a water/ethanol solution [23]. That orthorhombic structure consists of a di-hydrate [23]. Hence, the great problem is to understand why the chlorine atom in the hydrochloride species of Moris et al. is bonded to an H atom instead of the positively charged nitrogen atom of N–H of cationic species. The molecular formula of tacrine is $C_{13}H_{15}ClN_2$ and, its IUPAC name is 1,2,3,4-tetrahydroacridin-9-amine but, nowadays there are not specific studies justifying why the protonation of the cationic species takes place on the central ring of the N atom while the Cl atom is bonded to the N of NH_2 in the HCl species instead of the positively charged N–H group. So far, all possible theoretical structures of CA and HCl species of tacrine are unknown. For these reasons, in this work, two possible theoretical cationic and three hydrochloride structures of tacrine have been proposed, named forms I, II and III, which can be seen respectively in Fig. 1. The identifications of three rings in different colours are also presented in that figure. In this investigation, the structures of free base and those other proposed for the cation and hydrochloride species of tacrine were theoretically optimized in order to see which of all structures better reproduce the experimental infrared, Raman, ^{1}H NMR and UV–visible spectra. To achieve these purposes, the hybrid B3LYP method and the 6–311++G** and B3LYP/6-311G* basis sets have been used together with the scaled quantum force field (SQMFF) methodology to calculate the harmonic force fields and scaled force constants of the different species. This procedure has first allowed the determination of most stable structures of tacrine and, later, the complete vibrational assignments of all anhydrous species of tacrine. Good correlations were obtained among the theoretical results and the experimental ones while the predicted properties support the presence of form I CA and forms I and III of HCl species of tacrine. Besides, these results suggest that the CA form of tacrine is present in the solid phase and in solution, as it was also observed in other hydrochloride species [24–26]. For a better description and analysis of the species in all manuscript, we have called the free base FB, the cationic CA and the hydrochloride species HCl.

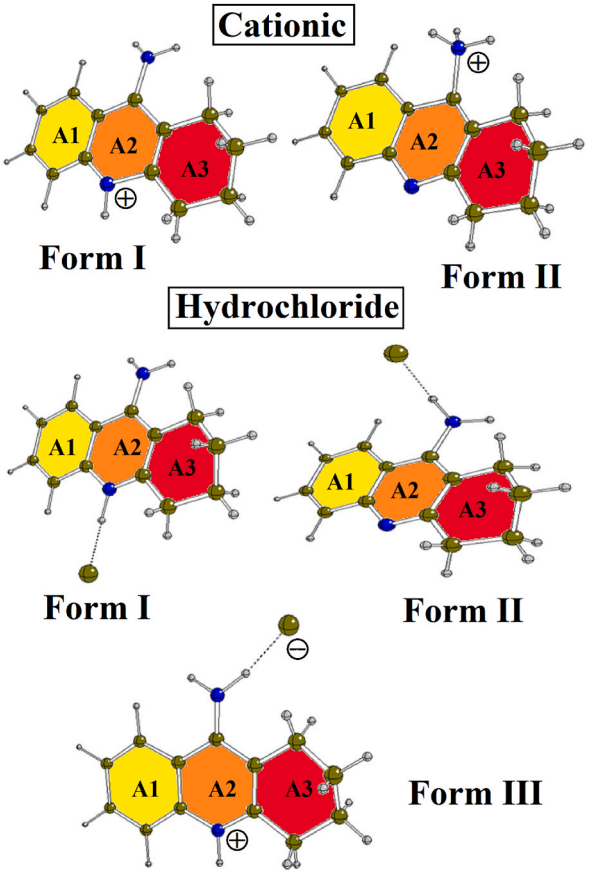

Fig. 1. Structures of two forms cationic (I and II) and three hydrochloride (I, II and III) species of tacrine with definitions of rings.

2. Material and methods

All calculations were made in gas phase and in aqueous solution with the Gaussian 09 program [27] and the functional hybrid B3LYP using the 6-31G*, 6-311G* and 6–311++G** basis sets [28,29]. In this study, it is necessary to clarify that the effect of dispersion was not considered because it generates lower energy values (less negative values) and, hence, less stable structures while all vibrational analyses should be performed taking into account the most stable structures. For instance, for the free base of tacrine when the WB97XD method was employed the energy value by using the B3LYP/6-311G* is −613.4756 Hartrees while with the WB97XD/6-311G* level of theory the value of energy is −613.2699 Hartrees. Hence, the B3LYP method was used for all calculations [30]. The initial structures of FB, forms I and II of CA and three forms HCl of tacrine were displayed with the *GaussView* program [31]. In aqueous solution, the integral equation-formalism polarizable continuum model (IEF-PCM) and universal solvation method (SMD) were employed [32–34]. The molecular volumes were computed with the Moldraw program [35]. Properties such as, atomic charges, bond orders, stabilization and topological energies were predicted with the NBO 5.1 and AIM 2000 programs [36–38] while the molecular electrostatic potentials and mapped surfaces were computed from the Merz-Kollman charges and graphed with the *GaussView* program [31,39]. Estimations of reactivities and behaviour of all species in the two media were performed using the frontier orbitals and equations of chemical potential, electronegativity, global hardness, global softness and global electrophilicity index [40, 41]. The harmonic force fields, normal internal coordinates and transferable scaling factors were computed with the SQMFF methodology and the Molvib program. As in similar species containing NH_2, CH_3 and NH_3^+ groups, symmetries C_{2v} and C_{3v} were considered for those groups [24–26]. To perform the vibrational assignments potential energy distribution (PED) contributions $\geq$10% and the experimental IR and Raman bands of tacrine in the solid phase were used [42–45] while the Raman spectra were corrected from activities to intensities to obtain better concordances [46]. Predicted ^{1}H and ^{13}C NMR spectra of species in aqueous solution with the GIAO method [47] were compared with the corresponding experimental obtained for tacrine in water deuterated (D_2O) [45]. Finally, the predicted electronic spectra for all species of tacrine in aqueous solution using the Gaussian 09 program [31] were compared with the corresponding experimental of tacrine hydrochloride monohydrate in methanol solution [45].

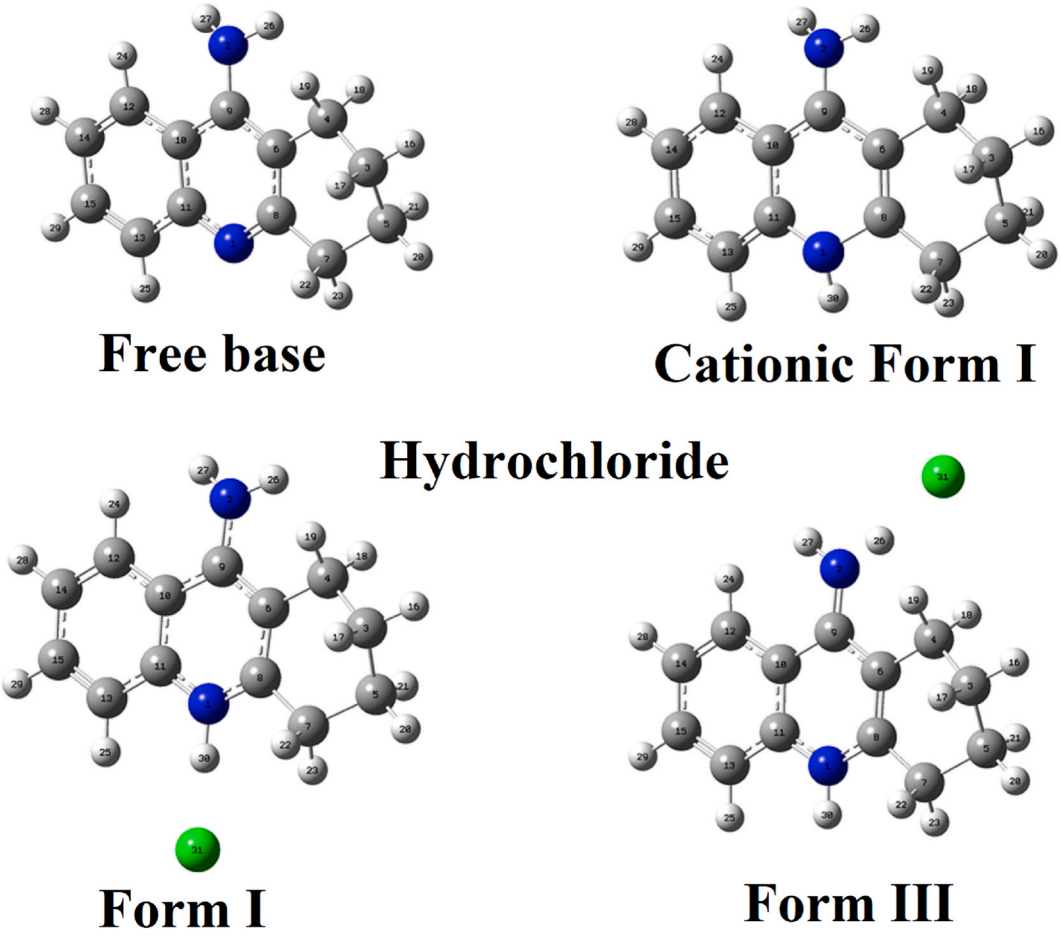

Fig. 2. Optimized structures of freebase, form cationic (I) and forms hydrochloride (I and III) species of tacrine and atoms labelling.

3. Results and discussion

3.1. Optimizations in different media

The optimized structures of FB, CA and HCl of anhydrous tacrine can be observed in Fig. 2 while the results obtained from the different calculations, including forms I and II of CA and the three forms of HCl species, are presented in Table 1. Figs. S1 and S2 show structures of two forms (I and II) of CA and the three forms (I, II and III) of HCl, respectively optimized with the hybrid B3LYP/6-311G* method. This latter method was used because the free base was optimized with the higher size 6–311++G** basis set but the frequencies at this level of theory were no obtained in order to check the nature of the reached stationary points. For this reason, FB was later optimized with the 6-31G* and 6-311G* basis sets evidencing positive frequencies with both levels of calculations and, hence, in Table 1, the symbol # is observed for FB with the 6–311++G** basis set in the column E_{ZPVE} indicating that the correction by ZPVE was not obtained at this level. Thus, to perform all optimizations and calculations corresponding to CA and HCl species the hybrid B3LYP/6-311G* method was directly used in order to compare the properties of FB with the corresponding to other species. Note that for the form III of HCl in gas phase the calculations with the 6–311++G** basis set was also included. The calculated total uncorrected and corrected by zero-point vibrational energy (ZPVE) are presented in Table 1 together with the molecular volumes and dipole moments values for all species in both media at different levels of theory. The results for HCl species show that the forms I and III present lower energy values in both media, decreasing the energy differences between them from 35.15 kJ/mol in gas phase to 5.51 kJ/mol in solution. The theoretical form I of HCl has lower energy value than form III but the experimental one observed corresponds to form III. But, those two forms of HCl could be present (see Fig. 2) because the energy value decreases in solution indicating that both forms could be present in this medium. Note that the form III of HCl corresponds to that experimental observed in solid phase by Moris et al. [23]. Table 1 shows that the form I of CA is the most stable in both media, hence, it presents lower energy values in the two media. We observed that the form II of CA and forms I and III of HCl in both media together with FB have higher dipole moment values and were calculated with the B3LYP/6-311G* method, especially in aqueous solution. In relation to molecular volumes, we observed that the FB with the 6-311G* basis set presents higher value (220.6 $Å^3$) than the other ones and, it is approximately similar to value predicted in solution (220.7 $Å^3$). However, the dipole moment value increases from 3.50 D in gas phase to 5.94 D in solution. Obviously, the CA and HCl species have higher dipole moments in the two media due to the added H and Cl atoms, respectively. The positions and orientations of dipole moment vectors for all species of tacrine in both media are given in Figs. S3 and S4. Carefully analysing the graphics from those two figures, we observed that the positions and orientations of vectors in the three species are different and, the directions and magnitudes of vectors change in considerable form for the FB and HCl species in solution while for the CA the magnitude of vectors remain practically constant in both media and only a slight change in the direction is observed in solution. In FB, the vector is oriented from A2 ring towards the NH_2 group. In both forms of HCl, different magnitudes, directions and orientations of vectors, are observed.

Table 1
Calculated total (*E*), dipolar moment (μ), volume (V) and population values of free base, cationic and hydrochloride species of tacrine in gas phase and aqueous solution by using the B3LYP method and different basis sets.

B3LYP METHOD				
FREE BASE				
GAS PHASE				
Basis set	*E* (Hartrees)	E_{ZPVE} (Hartrees)	μ (Debye)	V ($Å^3$)
6-31G*	−613.3470	−613.1002	3.38	221.0
6-311G*	−613.4756	−613.2300	3.50	220.6
6-311++G**	−613.5076	#	3.48	220.3
AQUEOUS SOLUTION				
6-31G*	−613.3615	−613.1149	5.58	221.2
6-311G*	−613.4919	−613.2466	5.94	220.7
CATIONIC				
GAS PHASE				
Form I/6-311G*	−613.8823	−613.6225	0.68	223.0
Form II/6-311G*	−613.8233	−613.5636	9.21	224.4
AQUEOUS SOLUTION				
Form I/6-311G*	−613.9638	−613.7043	0.68	222.6
Form II/6-311G*	−613.9328	−613.6723	14.05	223.6
HYDROCHLORIDE/6-311G*				
GAS PHASE				
Form I/6-311G*	−1074.3319	−1074.0737	14.25	247.2
Form II/6-311G*	−1074.3138	−1074.0586	3.94	250.0
Form III/6-311G*	−1074.3185	−1074.0598	16.39	246.9
Form III/6–311++G**	−1074.3524	−1074.0953	15.57	246.4
AQUEOUS SOLUTION				
Form I/6-311G*	−1074.3771	−1074.1183	22.06	249.7
Form II/6-311G*	−1074.3516	−1074.0918	12.74	250.3
Form III/6-311G*	−1074.3750	−1074.1155	20.42	248.7

#: Uncorrected by ZPVE due to that was not possible to obtain the frequencies calculations.

Thus, in the form I of HCl, the vector is oriented from the NH group towards the NH_2 group through of A2 ring and in the direction of C–N bond, as observed in Fig. S4 while in the forms III, from Fig. S4, the vectors follow approximately parallel trajectories to Cl···H–N bond but with different directions in the two media.

3.2. Solvation energies

In the species of tacrine, the presence of donor (N–H) and acceptor (N, Cl) groups of H bonds produce changes in the structures, volumes and, obviously different magnitudes, orientations and directions of the dipole moments vectors, and, in particular, when they are hydrated in aqueous solution. Consequently, the solvation energies are interesting parameters necessary to evaluate the different degrees of solvation of these species in a given medium. Here, the corrected solvation energies (ΔG_c) are calculated from the difference between the corrected solvation energies by ZPVE ($\Delta G^{\#}_{un}$) and by the non-electrostatic terms (ΔG_{ne}). The corrected solvation energies by ZPVE and by the total non-electrostatic terms of most stable FB, CA and HCl species of tacrine in aqueous solution by using the B3LYP/6-311G* method are presented in Table 2. For instance, for FB, the value of $\Delta G_c = -52.94$ kJ/mol is calculated as, $\Delta G_c = (\Delta G^{\#}_{un})-(\Delta G_{ne}) = -43.54 - 9.40 = -52.94$ kJ/mol. The ΔG_c values for all species of tacrine are compared with other species calculated by using the B3LYP method [24,26]. The C–NH_2 group is present in the free base species of tacrine and in amantadine and rimantadine [26,48] while in all alkaloids the characteristic groups are N–CH_3. Note that FB of tacrine (−52.94 kJ/mol) presents a higher value than the corresponding to the antiviral amantadine (−20.32 kJ/mol) while the value of form I of CA of tacrine is −229.98 kJ/mol and for the form II of CA the value is −298.91 kJ/mol. The two forms I and III of HCl present values of −132.49 and −162.02 kJ/mol, respectively. Hence, groups associated to CA and HCl species of tacrine (N–H^+ and N–H^+···Cl^-) are different from those related to amantadine (H–N^+-CH_3 and Cl^-···H–N^+-CH_3) and, for these reasons, different biological properties are observed in those species.

3.3. Structural study

Optimized parameters calculated for all forms and species of tacrine with the B3LYP/6-311G* method are compared in Table 3 with the corresponding experimental determined for the form III orthorhombic pseudopolymorph of tacrine HCl by Moris et al. by using X-ray diffraction [23]. Concordance among the theoretical and experimental values were analysed by means of the root-mean-square deviation values (RMSD). The deep analyses of results show that the form III of HCl in both media present better concordance and lower RMSDs in bond lengths and angles, as it is expected because this form HCl corresponds to that experimental observed in solid phase [23]. Thus, form III shows higher values in the H26–Cl31 distances in both media (2.363–1.898 Å) than the other form, being the rmsd value of this form in solution near to the experimental one (2.401 Å). In general, the bond lengths of form I present RMSD values in gas phase and solution of 0.184 and of 0.093 Å, respectively while form III shows lower RMSD values (0.172–0.069 Å). Analysing form I of CA, it is interesting to see that the N1–H30 distances in both media are higher than the corresponding to N2–H26 and N2–H27 of NH_2 group. In form I of HCl, the N1–H30 distances increase but the corresponding to NH_2 group remain practically without change. Thus, as we see later, the higher N1–H30 distance corresponds to the most labile H30 because it presents lower molecular electrostatic potential (MEP), for which, the Cl atom is added to the H30 of cationic species given the form I of HCl. In relation to the bond angles, the most important observation is that the bond in H26–N2–H27 angles present similar values in CA in both media while in form I of HCl the value is lower in gas phase than the predicted in aqueous solution. On the other side, the bond N2–H26–Cl31 angles show higher values in the form I of HCl, as compared with the form III of the same species. Here, the dihedral angles present the higher RMSD

Table 2
Corrected solvation energies by ZPVE and by the total non-electrostatic terms of free base, cationic and hydrochloride species of tacrine in aqueous solution by using the B3LYP/6-311G* method.

TACRINE[a]			
Solvation energy (kJ/mol)			
B3LYP/6-311G* method[a]			
Species	ΔG_{ZPVE}	ΔG_{ne}	ΔG_c
Free base	−43.54	9.40	−52.94
Cationic (Form I)	−214.56	15.42	−229.98
Cationic (Form II)	−285.12	13.79	−298.91
Hydrochloride (Form I)	−116.98	15.51	−132.49
Hydrochloride (Form III)[c]	−146.10	15.92	−162.02
B3LYP/6-31G* method			
Agents	Free base	Cationic	Hydrochloride
Amantadine[b]	−20.32	−273.24	−109.01
Morphine[b]	−60.91	−309.19	−144.74
Cocaine[b]	−71.26	−255.24	−138.14
Scopolamine[b]	−75.47	−310.34	−122.74
Heroin[b]	−88.67	−323.14	−161.94

[a] This work.
[b] From Ref. [26,48].
[c] The form III of HCl was only corrected by non-electrostatic terms (see text).

Table 3
Calculated geometrical parameters for the free base, cationic and hydrochloride tacrine species in gas and aqueous solution by using the B3LYP/6-311G* method compared with the experimental for the hydrochloride species of tacrine in solid phase.

B3LYP/6-311G*[a]									Exp[b]
Parameters	Free base		Cationic		Hydrochloride				
			Form I		Form I		Form III		
	Gas	Water	Gas	Water	Gas	Water	Gas	Water	
Bond lengths (Å)rowhead									
N1–H30			1.012	1.013	1.090	1.033	1.009	1.014	0.898
N1–C8	1.320	1.328	1.351	1.349	1.334	1.348	1.365	1.350	1.353
N1–C11	1.358	1.361	1.376	1.372	1.366	1.372	1.374	1.373	1.361
N2–H26	1.007	1.008	1.005	1.007	1.005	1.007	1.077	1.018	0.866
N2–H27	1.007	1.008	1.005	1.007	1.004	1.006	1.008	1.007	0.897
N2–C9	1.385	1.374	1.341	1.337	1.361	1.339	1.315	1.334	1.333
C9–C10	1.431	1.435	1.443	1.446	1.437	1.445	1.460	1.449	1.437
C9–C6	1.393	1.399	1.419	1.419	1.405	1.416	1.438	1.421	1.419
C6–C4	1.517	1.517	1.516	1.514	1.516	1.514	1.512	1.514	1.482
C10–C12	1.418	1.419	1.415	1.415	1.416	1.415	1.411	1.415	1.446
H26–Cl31					1.853	2.194	1.898	2.363	2.401
RMSD	**0.775**	**0.775**	**0.727**	**0.727**	**0.184**	**0.093**	**0.172**	**0.069**	
Bond angles (°)rowhead									
H30–N1–C8			118.1	118.2	119.1	118.9	118.3	118.4	115.5
H30–N1–C11			117.8	117.9	117.8	118.0	118.2	118.0	121.7
C8–N1–C11	118.2	118.0	124.0	123.7	122.9	123.0	123.3	123.4	122.6
C6–C9–C10	119.0	118.7	120.0	119.5	119.8	119.4	118.5	119.1	118.9
N2–C9–C10	120.0	120.5	120.3	120.3	119.9	120.5	121.1	120.2	120.0
N2–C9–C6	120.8	120.6	119.6	120.0	120.1	120.0	120.2	120.5	121.0
H26–N2–H27	112.2	112.6	116.3	116.6	115.4	116.4	111.7	114.8	112.9
N2–H26–Cl31					177.9	176.6	166.8	153.6	160.9
RMSD	**82.2**	**82.2**	**56.9**	**56.9**	**6.4**	**6.4**	**6.0**	**2.7**	
Dihedral angles (°)rowhead									
C9–N2–H26–Cl31					−124.2	−169.9	154.4	179.6	−164.1
N2–C9–C6–C8	−178.9	−179.4	−176.8	−178.0	−178.0	−176.0	−175.2	−177.5	−176.9
N1–C8–C6–C4	−178.8	−179.6	179.7	179.8	−179.3	179.6	178.7	−179.7	178.9
N1–C11–C10–C12	−178.5	−179.3	179.9	179.2	−179.0	−179.5	−179.5	179.9	−179.9
N1–C8–C7–C5	159.9	160.4	161.9	161.6	161.1	162.0	163.9	161.9	164.5
N1–C11–C13–C15	179.3	179.6	−179.8	−179.3	179.6	179.8	179.7	−179.9	−165.9
RMSD	**213.7**	**214.0**	**161.5**	**161.3**	**203.8**	**141.2**	**191.9**	**250.5**	

[a] This work.
[b] Ref [23] for orthorhombic pseudopolymorph for tacrine hydrochloride.

values having the CA species the lower values in both media together with the form I of HCl. Both HCl forms show important changes in solution, thus the N1–C8–C6–C4 angle of form I change from negative in gas phase to positive in solution while the form III shows changes of signs in the dihedral N1–C8–C6–C4, N1–C11–C10–C12 and N1–C11–C13–C15 angles when the medium from gas phase to solution changes. Low RMSD values observed in bond lengths and angles for all species of tacrine suggest that their structures can be used to perform the corresponding vibrational assignments.

3.4. Atomic charges, molecular electrostatic potential (MEP) and bond orders

In this work, the analyses of atomic charges, molecular electrostatic potential (MEP) and bond orders are very important to elucidate and understand why the form III of HCl experimentally exists when, theoretically, the most stable is form I. Hence, only those charges, MEPs and bond orders corresponding to the C atoms of A2 ring and to the N and H atoms of NH and NH_2 groups were considered because those atoms play very important roles in their properties. Thus, atomic Merz-Singh-Kollman (MK), Mulliken (MU) and natural population (NPA) charges were calculated for all stable species in both media with the B3LYP/6-311G* method. These results for FB, form I of CA and forms I and III of HCl are summarized in Table S1 while in Figs. S5 and S6 the variations observed in the cationic and two forms of HCl are shown when the medium change from gas phase to aqueous solution. In Table S1 the molecular electrostatic potential (MEP) and bond orders are also presented, expressed as Wiberg indexes. First of all, the atomic charges for FB are analysed from Table S1. The analyses show that the three MK, MU and NPA charges on N atoms are negatively charged having the N1 lower values than N2 while the higher MU values are observed on N2 in both media. In solution, the three charges on N1 probably increase because its atom is protonated in this medium forming the CA species. In CA, the MK and NPA charges on N atoms decrease while the MU increase in both media, as descripted in Table S1 and observed in Fig. S4. On the H30, H26 and H27 atoms of this species three charges with similar values are observed while on the C6 and C10 atoms negative values are observed. On the contrary, the C8, C9 and C11 atoms present positive values where the higher NPA charges are observed on C11 atoms in both media. In relation to HCl, Fig. S6 shows clear differences between both forms I and III in the two media. Analysing first the two forms in gas phase, on N1 of form I less negative MK and NPA values are observed than the form III while on N2 of form I the MU value is more negative, as compared with form III. In solution, the three charges on N2 of form III present different values while in form I only the MU charges are different from

the other ones. Other important difference is observed in the three charges on C6 in solution because in the two forms of HCl the values are practically similar but in the gas phase the MK charge is more negative than the other ones. But, higher differences are observed in charges on H26, H27 and H30 because in the form III in solution the three charges on H30 present the same values while in form I only the charges on H26 and H27 are similar but, in form III the MK charge on H26 is different from other two, as it is expected because in this form the H26 is bonded to Cl31.

Evaluating the MEP values from Table S1 [39], a less negative MEP value is observed on H30 of CA indicating that this atom is the most labile in both media. However, in form I of HCl, the H30 atoms in both media have high negative MEPs values, as compared with H26 and H27 while on H26 of form III in both media the most negative MEPs values are observed. These results indicate that H30 is the most labile in the form III while in form I the most labile is the H27. When the mapped MEP surfaces of more stable species of tacrine are illustrated in Fig. S7, it is observed that FB presents the lower MEP value (±0.053 a.u.) in gas phase while in the form III of HCl the higher value (±0.095 a.u.). In FB, the strong red colour is located on N1 while on H26 and H27 strong blue colours indicate the nucleophilic and electrophilic regions where the reactions with potential electrophils and nucleophils take place, respectively. In the two forms of HCl the nucleophilic sites are located on Cl atoms but in the form I the electrophilic sites are located on both H of NH_2 group while in the form III on H27 and H30 of NH_2 and NH groups. As expected, the entire MEP surface of CA is completely blue because this species is positively charged and evidence typical electrophilic region.

When the bond orders (BO) totals by atom, expressed as Wiberg bond index, are analysed from Table S1, we can see that in FB the two N atoms present low values and where N1 has the lower value while in CA this atom has higher values in both media. In form III of HCl, N2 presents higher BO values in the two media than form I because the H26 of NH_2 is bonded to Cl31 while the H26 present lower values in form III than the other one. Here, the decrease of BO of Cl31 in form III of HCl, from 0.328 in gas phase to 0.145 in solution could explain the enlargement of H26···Cl31 bond, as a consequence of its hydration. In the same way, the BO of H26 decreases from 0.830 in gas phase to 0.803 in solution. If the Wiberg bond index matrix in the NAO basis are considered specifically for the H26···Cl31 bond in both forms of HCl, it is observed that in the form I the BO decreases from 0.2499 in gas phase to 0.1304 in solution while in the form III it decreases from 0.2175 to 0.0825 in solution. Hence, in the form III the bond is clearly ionic while in the form I that bond can be considered partially ionic.

3.5. Stabilities using NBO and AIM calculations

Probable intra-molecular and H bonds interactions due to NH_2 and NH groups present in all species of tacrine have been studied and analysed by using NBO and AIM calculations with the NBO and AIM 2000 programs, respectively [36–38]. Hence, evaluating first the donor-acceptor energy interactions with the Second-Order Perturbation Theory Analysis of Fock Matrix in NBO Basis, the main delocalization energies for FB, form I CA and forms I and III of HCl species of tacrine in both media by using B3LYP/6-311G* calculations are presented in Table S2 [36]. These results have evidenced a total of seven different transitions distributed of the following form: $\pi \rightarrow \pi^*$ transitions for the three species in the two media, with exception of the form I CA; $\pi \rightarrow n^*$ transitions only for the form I CA; $n \rightarrow \sigma^*$ transitions for all species, with exception of form I HCl; $n \rightarrow \pi^*$ transitions for all species, with exception of form III HCl; $\pi^* \rightarrow \pi^*$ transitions only for the forms I and III HCl and, $\sigma \rightarrow n^*$ and $n \rightarrow n^*$ transitions only for the form I of HCl in both media. The total energies of these transitions show that form I of HCl is the most stable species in both media due to higher energy values than the other ones and, then the form III of HCl in both media. The stability order observed for the most stable species of tacrine is the following: form I HCl > form III HCl > form I CA > FB. FB and CA species evidence higher stability or higher energy values in solution while the HCl species are less stable in this medium. Thus, the CA species is probably the most stable in solution due to its higher hydration, as its higher solvation energy suggests. This latter resulted was also observed for rimantadine and amantadine [26,48].

Afterwards, the interactions in all species of tacrine were also predicted by means of the topological properties have been calculated with the AIM 2000 program [37,38]. Thus, the electron density, the Laplacian values and the $|\lambda 1|/\lambda 3$ ratio are calculated in the bond critical points (BCPs) and in the ring critical points (RCPs). All these calculations were performed at the B3LYP/6-311G* level of theory and they are presented in Table S3 together with the distances of new H bonds. Here, with the eigenvalues of the Hessian matrix *(λ1, λ2, λ3)* the $|\lambda 1|/\lambda 3$ ratios are calculated. When the interaction is ionic or polar covalent interactions the ratio $\lambda 1/\lambda 3 < 1$ and $\nabla^2\rho(r) > 0$ (closed-shell interaction). Details of the molecular models for FB, form I CA and forms I and III HCl species of tacrine in gas phase with the geometries of BCPs and RCPs are presented in Fig. S8. Analyses of these results from Fig. S8 show that FB presents a new H bond: N2–H27···H24 and a new RCP named RCPN while the other RCP1, RCP2 and RCP3 belong to the A1, A2 and A3 rings, respectively. The form I CA show an H bond: C12–H24···H27 with the new RCPN. Both forms of HCl, III, and I evidence three new H bonds but with different characteristics, thus, the form I shows that new C13–H25···Cl31 and N1–H30···Cl31 bonds given the RCPN1 while the C12–H24···H27 generate the RCPN2. In the form III, RCPN1 is generated by the N2–H26···Cl31 and C4–H18···Cl31 bonds while the RCPN2 by the C12–H24···H27 bond. Analyzing the values of topological properties of three rings from Table S3, we observed that the densities of A1 and A3 rings show few changes in the three species while the A2 ring present different values in FB, CA and HCL. Thus, A2 in FB shows a higher density value (0.0219 a.u.) while the value decreases in CA to 0.0202 a.u. and, later, increase in the form I of HCl. On the contrary, the form III HCl evidences the lower density value (0.0198 a.u.) in gas phase. Both forms of HCl in gas phase show three H bonds, which remains in solution in the form I while in the form III, the number diminish to two. Hence, in solution form III is less stable while in gas phase both forms are stable. In relation to the distances, the H bonds of form III of HCl present lower values in solution than the corresponding to the form I and, therefore, the topological properties present higher values in form III. Here, a very important result is observed in the topological properties of new N1–H30···Cl31 and N2–H26···Cl31 bonds of forms I and III of HCL, respectively. Thus, the higher values observed in the topological properties for the form III in the two media, as compared with the form I, could justify the higher ionic character of form III which was experimentally observed in the solid phase and in solution. The

strong N2–H26···Cl31 interaction justifies the higher stability of form III in both media, showing in solution $\rho(r) = 0.0194$ a.u., $\nabla^2\rho(r) = 0.0524$ a.u. and $|\lambda 1|/\lambda 3$ ratio = 0.2162 a.u. (see Table S3). Here, the longer distance of N1–H30–Cl31 bond in solution evidence its transformation of covalent to ionic in the form I of HCl species (from 0.2499 in gas phase to 0.1304 in solution) while in form III the decrease is observed for the N2–H26···Cl31 bond from 0.2175 in gas phase to 0.0825 in solution. Hence, the BO of Cl31 is higher (0.1449) in form III in solution than in form I in the same medium (0.1304). Obviously, as HCl is a salt in solution is in its cationic form. Then, the form III of HCl in solution is less stable and presents higher ionic character.

3.6. Reactivity and behaviours in different media

Gap values, calculated as the differences between the frontier HOMO-LUMO orbitals, are useful parameters to predict reactivities and behaviours of a species in diverse media by using different descriptors [40,41]. Here, the behaviours of FB, form I CA and forms I and III of HCl species of tacrine are predicted in both media with the gap values and the following descriptors: (μ), (χ), (η), (S) and (ω). The equations used to calculate these descriptors using the hybrid B3LYP/6-311G* level of theory can be seen in Table S4 [40,41]. Note that in that table they are compared with the reported for antiviral rimantadine and amantadine agents [26,48]. Evaluating the gap values, we observed the lower values for both forms of HCl, thus, the value for form I in gas phase of 3.0450 eV decreases in solution to 2.2123 eV while for the form III decreases from 2.4572 eV to 1.3877 eV. Hence, form III in solution is more reactive than other ones while the FB species is the less reactive in both media. Obviously, FB in both media have higher (η) values (4.5443/4.5008 eV) because there are less reactive species while the HCl species are associated to higher (S) values because they are the most reactive ones. Here, a very interesting result is observed for CA because this species is positively charged and present high (ω) values in both media (14.0373/13.9644 eV), as expected. From Table S4 it is easy to see that both forms of HCl are more reactive than the corresponding to rimantadine and adamantine because the gap values for these two latter species are around 5.4036 and 4.1116 eV [26,48]. For the same reasons, the FB and CA species of those two antivirals species have higher gap values and, hence, they are less reactive than the corresponding to tacrine.

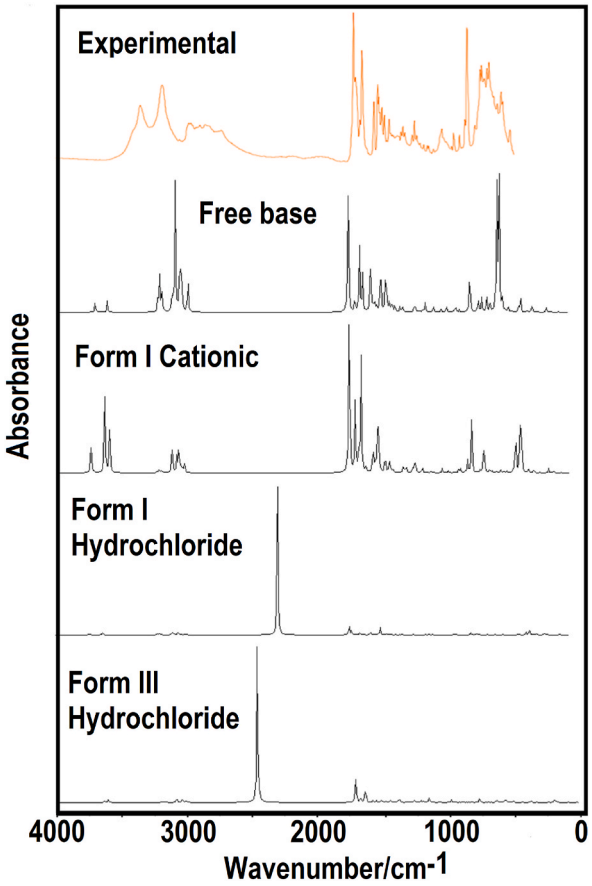

Fig. 3. Experimental Infrared spectra of hydrochloride species of tacrine in solid phase [45] compared with the predicted for free base, cationic (I) and hydrochloride (I and III) species of tacrine in gas phase by using the hybrid B3LYP/6-311G* method.

3.7. Vibrational study

In this work, the structures of FB, form I CA and forms I and III HCl of tacrine have been optimized by using hybrid B3LYP/6-311G* calculations with C_1 symmetries and, hence, the expected number of normal vibration modes for each species are 81, 84 and 87, respectively. Fig. 3 shows the experimental infrared spectrum of tacrine, as HCl species in the solid state, compared with the corresponding predicted for the three species in the gas phase [45]. Note that the very strong IR bands predicted for the form I of HCl by B3LYP/6-311G* and SQM calculations at 2263 and 2171 cm^{-1}, respectively and, for the form III at 2467 and 2365 cm^{-1}, respectively are not observed with the same intensities in the experimental IR spectrum. Fig. S9 shows the experimental transmission infrared spectrum of tacrine in the solid phase taken from Ref. [45] where the strong IR band at 776 cm^{-1} is observed with lower intensity. Fig. 4 displays the experimental IR spectrum of 1,2,3,4-Tetrahydro-9-acridinamine, monohydrochloride with the three predicted forms of HCl showing that the absence of these strong IR bands in the 2500-2100 cm^{-1} region of experimental spectrum simply indicates that in the solid phase the compound is not present as hydrochloride but as a free base or in its cationic form I. On the other, the comparisons presented in Fig. 5 for the two cationic forms show that the most stable form I is present in the solid phase because its predicted IR spectrum is similar to the experimental one. However, when the predicted Raman spectra for all tacrine species in gas phase are compared with the corresponding experimental one of Fig. 6, we observed that those two strong IR bands between 2500 and 2100 cm^{-1} in the Raman spectrum are observed with less intensities indicating that these forms of HCl are not present in solid phase [45]. The theoretical Raman spectra predicted in activities were corrected to intensities [46]. The vibrational assignments were performed with the calculated harmonic force fields using the SQMFF methodology and the Molvib program [42–44]. Recommended transferable scaling factors were employed together with the normal internal coordinates [42]. In this case, we have considered only PED contributions ≥10%. Table 4 shows observed and calculated wavenumbers and assignments for FB, form I CA and forms I and III HCl of tacrine in gas phase. The IR and Raman bands observed in the 2827–2686 and 720-693 cm^{-1} regions confirm the presence of form I CA of HCl in the solid phase because for the other species bands are not predicted in that region. Below, discussions of assignments for some groups are presented by regions.

3.7.1. Band assignments

4000–2000 cm^{-1} region. Stretching modes of NH_2, CH_2 and C–H groups of three species of tacrine are assigned in this range [24–26,48]. In this way, the shoulder and IR band at 3378 and 3330 cm^{-1} are assigned to the two NH_2 stretching modes of FB and form I of HCl while the antisymmetric mode of form III of HCl, predicted to 3486 cm^{-1}, is also assigned to the shoulder at 3378 cm^{-1}. In the form I of CA those two modes are predicted to 3311 and 3211 cm^{-1} and, hence, they are assigned to 3330 and 3163 cm^{-1}, as descripted

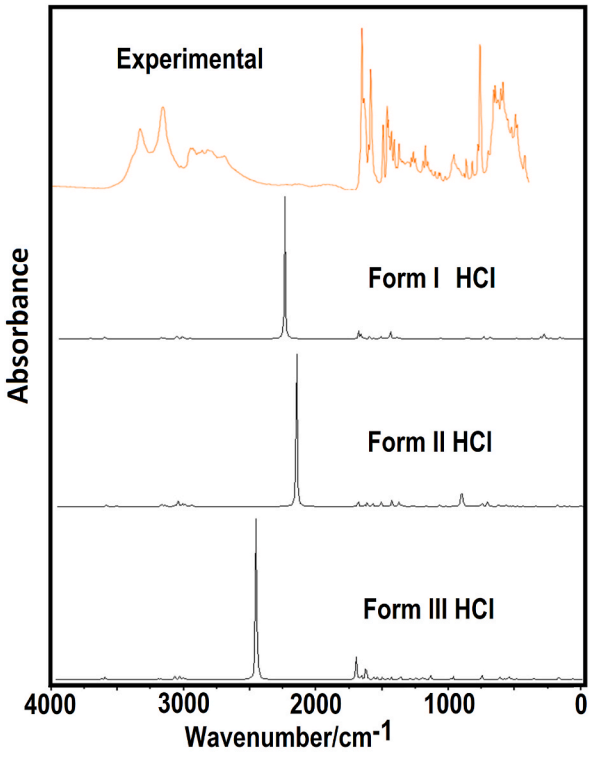

Fig. 4. Experimental Infrared spectra of hydrochloride species of tacrine in solid phase [45] compared with the predicted for hydrochloride species (I, II and III) of tacrine by using the hybrid B3LYP/6-311G* method.

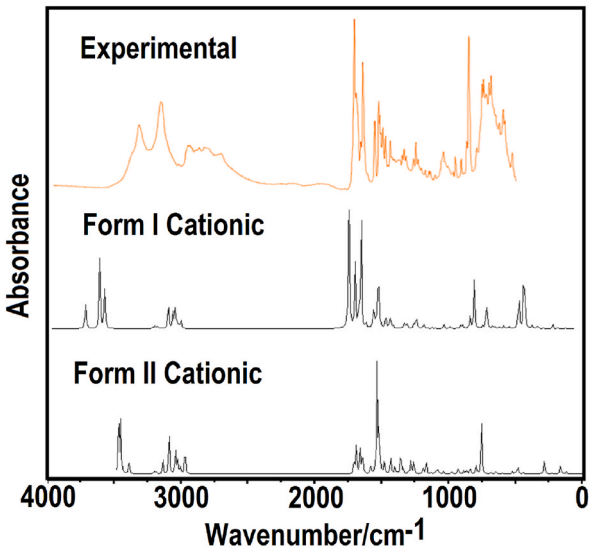

Fig. 5. Experimental Infrared spectra of hydrochloride species of tacrine in solid phase [45] compared with the predicted for cationic species (I and II) of tacrine by using the hybrid B3LYP/6-311G* method.

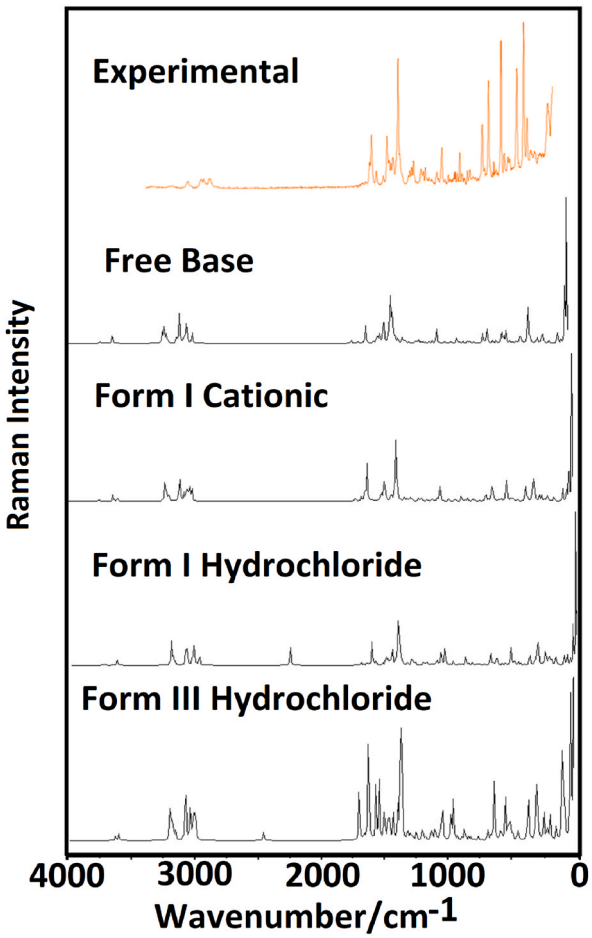

Fig. 6. Experimental Raman spectra of hydrochloride species of tacrine in solid phase [45] compared with the predicted for free base, cationic (I) and hydrochloride (I and III) species of tacrine in gas phase by using the hybrid B3LYP/6-311G* method.

Table 4
Observed and calculated wavenumbers (cm^{-1}) and assignments for the free base, form I cationic and forms I and III hydrochloride species of tacrine.

Exp[c]		B3LYP/6-311G* Method[a]							
		Free base		Form I Cationic		Form I Hydrochloride		Form III Hydrochloride	
IR	Raman	SQM[b]	Assignments[b]	SQM[b]	Assignments[b]	SQM[b]	Assignments[b]	SQM[b]	Assignments[b]
3378sh		3533	ν_aNH_2	3347	νN1-H30	3576	ν_aNH_2	3486	ν_aNH_2
3330 m	3277vw	3443	ν_sNH_2	3311	ν_aNH_2	3476	ν_sNH_2	3462	νN1-H30
3163s	3242vw			3211	ν_sNH_2			3072	νC14-H28
3089sh	3098vw							3060	νC15-H29, νC12-H24
3067sh		3065	νC13-H25			3068	νC15-H29	3051	νC14-H28, νC12-H24,νC15-H29
		3052	νC14-H28	3042	νC12-H24	3059	νC13-H25,νC14-H28		
		3036	νC15-H29	3011	νC15-H29	3051	νC15-H29,νC13-H25		
3028vw		3026	νC12-H24			3037	νC12-H24	3034	νC13-H25
	2971w	2957	ν_aCH_2(C7)	2970	νC14-H28	2962	ν_aCH_2(C7)	2962	ν_aCH_2(C3)
2950 m		2938	ν_aCH_2(C3)	2959	νC13-H25	2956	ν_aCH_2(C5)	2956	ν_aCH_2(C4)
2924 m		2936	ν_aCH_2(C5)			2949	ν_aCH_2(C3)	2953	ν_aCH_2(C5)
						2912	ν_sCH_2(C3)	2923	ν_sCH_2(C4)
		2902	ν_sCH_2(C3)	2905	ν_aCH_2(C5)	2905	ν_sCH_2(C7)	2919	ν_sCH_2(C5)
2888sh		2892	ν_sCH_2(C5)	2888	ν_aCH_2(C4)	2898	ν_sCH_2(C5)	2905	ν_aCH_2(C7)
	2871w	2886	ν_aCH_2(C4)	2885	ν_aCH_2(C3)	2892	ν_aCH_2(C4)	2892	ν_sCH_2(C3)
2866 m		2882	ν_sCH_2(C7)	2869	ν_sCH_2(C5)			2881	ν_sCH_2(C7)
	2851w	2840	ν_sCH_2(C4)	2855	ν_sCH_2(C3)	2856	ν_sCH_2(C4)		
2827 m	2807w			2822	ν_sCH_2(C4)				
2792 m	2794sh			2762	ν_sCH_2(C7)				
2700 m	2757vw			2686	ν_aCH_2(C7)				
2319vvw	2333vvw							2365	ν_sNH_2
2250vvw						2172	νN1-H30		
1665vs		1640	δNH_2	1630	νC6-C8	1655	βN1-H30	1627	δNH_2,βN1-H30
1650s				1610	δNH_2	1633	δNH_2	1626	δNH_2
1615s	1573 m	1608	νC13-C15, νC12-C14			1608	νC13-C15	1594	νC13-C15, βN1-H30
1600s	1562s	1573	νC6-C9	1555	νC11-C13	1571	νC10-C11,νC12-C14	1586	νC6-C8
1506s	1523w	1549	νC14-C15, νC10-C11	1521	νC10-C12	1543	νC6-C9	1531	νC6-C8, νN1-C8
1475s	1475w	1489	νC14-C15, βC12-H24	1484	βN1-H30	1492	νC14-C15,βC15-H29	1499	νN2-C9
1466s	1468w	1453	δCH_2(C3)	1454	νC12-C14	1452	δCH_2(C5),δCH_2(C3)	1466	βC12-H24
1459 m		1449	βC15-H29	1445	δCH_2(C7)	1450	βC14-H28,βC15-H29	1450	δCH_2(C5)
1442s	1442s	1442	δCH_2(C5)	1437	δCH_2(C4)	1444	δCH_2(C5),δCH_2(C3)	1444	δCH_2(C3)
	1438sh	1437	δCH_2(C4)	1430	δCH_2(C3)	1435	δCH_2(C4)	1438	βC15-H29,βC14-H28
1420 m	1425w	1424	δCH_2(C7)	1422	δCH_2(C5)	1420	νN2-C9	1418	δCH_2(C7)
1416sh	1411w	1413	δCH_2(C7), βC12-H24			1418	δCH_2(C7)	1414	$wagCH_2$(C4), νC6-C9
1386 m	1386w			1402	βC15-H29, βN1-H30	1393	$wagCH_2$(C4)	1408	δCH_2(C4)
1375sh	1372sh	1380	$wagCH_2$(C4), νC6-C8			1384	$wagCH_2$(C7)	1380	$wagCH_2$(C7), $wagCH_2$(C4)
1363sh		1370	$wagCH_2$(C5) $wagCH_2$(C3)	1367	νC4-C6	1363	$wagCH_2$(C3)	1363	$wagCH_2$(C3)
	1355vs	1358	$wagCH_2$(C3)	1352	$wagCH_2$(C5)	1360	$wagCH_2$(C5), $wagCH_2$(C3)		
1350sh	1355vs	1351	$wagCH_2$(C7)	1348	$wagCH_2$(C3)	1355	$wagCH_2$(C5)	1355	$wagCH_2$(C5)
	1346sh	1351	$wagCH_2$(C5)	1341	$wagCH_2$(C4), $wagCH_2$(C7)	1342	$wagCH_2$(C4)	1345	$wagCH_2$(C7)
1322w	1333sh	1330	νC10-C11	1321	νC9-C10			1331	νC10-C11,νC12-C14
1307w		1309	νN1-C8	1295	νC10-C11	1309	νN1-C8	1296	ρCH_2(C4), ρCH_2(C5)
1294w		1276	βR_1(A2), βC12-H24	1283	νC6-C9	1278	βC12-H24,βR_1(A2), νC11-C13	1280	βR_1(A2)
1276 m	1274w	1266	ρCH_2(C4)	1260	ρCH_2(C5)	1270	νN1-C8, ρCH_2(C4)	1258	ρCH_2(C7), ρCH_2(C4)
1261w	1250w	1245	ρCH_2(C7)			1251	ρCH_2(C7), ρCH_2(C7)	1247	νN1-C11,νC10-C12
	1239w	1224	νN1-C11, νC10-C12	1236	νC6-C9, ρCH_2(C4)	1241	νN1-C11, νC10-C12	1224	νN1-C8
1207w	1217sh			1217	ρCH_2(C7), ρCH_2(C3)				
1186 m	1180w			1187	νN1-C11	1186	βC14-H28	1185	ρCH_2(C5),ρCH_2(C3)

(*continued on next page*)

Table 4 (*continued*)

Exp[c]		B3LYP/6-311G* Method[a]							
		Free base		Form I Cationic		Form I Hydrochloride		Form III Hydrochloride	
1169w		1178	βC14-H28, νC4-C6			1178	ρCH_2(C3), wagCH_2(C4)	1177	βC14-H28
	1160w	1165	ρCH_2(C5)	1160	νC7-C8	1161	βC15-H29,βC13-H25	1159	βC15-H29,βC13-H25
1147w	1145w	1151	ρNH_2	1157	ρNH_2	1144	ρCH_2(C5),ρCH_2(C3)	1145	ρCH_2(C3), ρCH_2(C5)
				1150	βC12-H24				
1138sh	1138sh	1134	ρCH_2(C5), ρCH_2(C3)						
		1121	βC13-H25, νC9-C10	1126	νN1-C8, βC14-H28	1123	ρNH_2,νC9-C10		
				1124	βC15-H29, βC13-H25			1119	νC9-C10, νC11-C13
1114w	1117w	1103	νC11-C13	1112	ρCH_2(C4)	1110	βR_1(A3)	1107	ρNH_2
1086w	1097w	1076	νN2-C9 νC7-C8			1085	νC7-C8	1081	νC7-C8
1078w	1062sh			1056	βR_1(A3)	1077	δN1-H30-Cl31		
1038w	1056w	1047	νC3-C5	1045	νC3-C5 νC5-C7	1047	νC3-C,5νC3-C4	1042	νC3-C5, νC3-C4
1012sh	1018s	1011	τwCH_2(C3) τwCH_2(C4)	1033	νN2-C9	1016	νC14-C15	1022	νC14-C15
		1010	νC14-C15			1012	τwCH_2(C3),τ wCH_2(C5)	1010	τwCH_2(C5),τwCH_2(C3), τwCH_2(C7)
1000sh	994w			1008	νC13-C15 νC14-C15	1004	γC15-H29 γC13-H25		
985sh	970w	980	γC15-H29 γC13-H25	1001	τwCH_2(C7) τwCH_2(C4)			975	γC15-H29, γC14-H28
973 m		958	νC3-C4 νC5-C7			960	νC3-C4 νC5-C7	964	νC5-C7, νC3-C4
966sh	960w			942	νC5-C7 νC3-C4	941	γC14-H28	941	τwN2-H26 wagNH_2
946sh	940vw	929	γC14-H28					927	γC12-H24
900vw	918w	903	βR_1(A1)	903	βR_1(A1)	902	βR_1(A1)	899	βR_1(A1)
880 m	885s	867	βR_1(A3)	873	γC14-H28 γC12-H24	868	βR_1(A3)	866	βR_1(A3)
874sh	868w	860	γC12-H24, τR_1(A2)			862	γC12-H24		
	848w	854	νC3-C5	854	βR_1(A3)	854	νC3-C5	852	νC3-C5
836 m		842	τwCH_2(C7) τwCH_2(C5)	845	τwCH_2(C7) τwCH_2(C4) τwCH_2(C3)			843	γC13-H25
	827w			841	νC3-C5	838	τwCH_2(C4),τ wCH_2(C7)	832	τwCH_2(C4)
793sh	805w	796	τR_1(A2), γC9-N2	798	γC12-H24, τR_1(A3)	794	τR_1(A2)	793	τR_1(A2)
776vs	778w	782	τR_1(A2)	786	νC3-C5	782	τR_1(A2)	783	γC9-N2,τR_1(A2)
760sh	760w	758	τR_1(A3)	768	γC13-H25	757	τR_1(A3),γC12-H24	754	γC15-H29,τwCH_2(C4)
	744w	753	γC12-H24	762	τwCH_2(C5)	746	γC14-H28,γC12-H24	741	τR_1(A3), γC14-H28
	720sh			730	wagNH_2				
717 m	710s			715	τR_1(A3)				
	693w			703	γN1-H30				
676s	679vw	680	τR_1(A3), γC9-N2			688	νC4-C6	693	τR_1(A3) νC4-C6
662s	662s	669	τR_1(A3)			670	τR_1(A3), γC9-N2	670	τR_1(A3)
643s	650sh	656	βR_3(A3)	646	βR_3(A3)	652	βR_3(A3)	656	βR_3(A3)
621s	621w	620	βR_2(A3), τR_2(A2)	636	γC15-H29	615	βR_2(A3)	603	βR_2(A3)
604s	601w	592	βR_2(A3)	601	βR_1(A1) γN1-H30	590	βR_2(A3), βC9-N2	601	γC9-N2
573sh	576sh			576	βR_2(A3)			567	βR_3(A3), $\tau_w NH_2$
	566vs	553	τR_2(A2), βR_3(A3)	555	βR_1(A2)	553	βR_3(A3) τR_2(A2)	555	γN1-H30
540 m	539w	542	wagNH_2	538	τR_1(A2)	525	τR_3(A3)	536	γN1-H30,τR_2(A2)
511s	511w	523	wagNH_2 τR_3(A3)	525	τR_3(A3)			523	τR_3(A3)
499s	499w	501	βR_3(A1) βR_3(A2)			500	βR_3(A1) βR_3(A2)	497	βR_3(A1) βR_3(A2)

(*continued on next page*)

Table 4 (*continued*)

Exp[c]		B3LYP/6-311G* Method[a]							
		Free base		Form I Cationic		Form I Hydrochloride		Form III Hydrochloride	
487sh	492sh	481	βR_2(A1)	480	βR_2(A1)	483	βR_2(A1)	483	βR_2(A1)
			βR_2(A2)		βR_1(A1)		βR_2(A2)		βR_1(A1)
444 m	444s	449	ButC10-C11	468	τR_2(A3)	451	τR_2(A3)		
					ButC10-C11				
422sh	427sh	428	βR_2(A2)	443	ButC10-C11	427	βR_2(A2),βR_2(A1)	424	βR_2(A2)
	407sh			417	βR_3(A2)βR_2(A2)			416	τR_2(A3), ButC10-C11
	391vs	375	βR_3(A1)			374	βR_3(A1) $\tau_w NH_2$	366	βR_2(A2),βC9-N2
	367s	348	$\tau_w NH_2$	356	βR_3(A1)	366	$\tau_w NH_2$	357	βC9-N2
	336w	311	τR_1(A1)			325	βC9-N2		
			τR_3(A3)						
	309w	306	ButC6-C8	303	τR_1(A1)	313	τR_1(A1)	309	τR_1(A1)
			τR_2(A3)		βC9-N2				
	299sh			298	βC9-N2	299	wagNH_2	286	ButC6-C8
					τR_1(A1)				
	284sh			285	ButC6-C8	287	ButC6-C8		
					τR_2(A3)				
	273sh	279	τR_3(A1)			275	τR_3(A1)		
	265w	264	$\tau_w NH_2$	266	τR_2(A3)			265	τR_3(A1)
			βC9-N2		ButC6-C8				τR_2(A2)
	242w	231	βR_2(A1)	242	τR_3(A1)	245	νH30-Cl31	226	βR_2(A1)
					τR_3(A1)		βR_2(A1)		
	206s			205	$\tau_w NH_2$	180	νH30-Cl31	173	νH26-Cl31
	173sh	161	τR_2(A1)	163	τR_3(A3)	157	ButC10-C11	156	τR_2(A1)
					τR_1(A2)				
				143	τR_2(A1)				
		129	τR_2(A1)			126	τR_1(A2)	113	ButC6-C8
			τR_2(A2)				τR_2(A1)		τR_3(A1)
				110	γC9-N2				
		91	τR_3(A2)	96	τR_3(A1) τR_3(A2)	99	τR_3(A2)	99	τR_3(A2)
		68	τR_2(A2)			69	τR_2(A1)τR_2(A2)	71	δN2-H26-Cl31
						67	τwN1-H30	54	τR_2(A2), $\tau_w NH_2$
				39	τR_2(A2)	42	γN1-H30		
								16	wagNH_2
									τwN2-H26,$\tau_w NH_2$

Abbreviations: ν, stretching; β, deformation in the plane; γ, deformation out of plane; wag, wagging; τ, torsion; β_R, deformation ring τ_R, torsion ring; ρ, rocking; τw, twisting; δ, deformation; a, antisymmetric; s, symmetric; (A_1), Ring1; (A_2), Ring2; (A_3), Ring3, [a]This work, [b]From scaled quantum mechanics force field; [c]From Ref [45].

in Table 4. The symmetric mode of form III of HCl is predicted with great intensity to 2365 cm^{-1} because the N2–H26 bond of NH_2 group is bonded to Cl atom and, for this reason, that vibration mode is associated to the very weak band at 2319 cm^{-1}. In the form I of HCl the N1–H30 stretching is also predicted with intense to 2172 cm^{-1} and, it is assigned to the very weak band at 2250 cm^{-1}. The absence of these strong bands in the experimental spectrum indicates that both forms are not observed in the solid phase as hydrochloride species but as cationic ones. Similar observations were reported for analogous species [24–26,48]. Note that the shoulders and IR and Raman bands between 3163 and 2950 cm^{-1} are associated to C–H stretching modes of all species of tacrine while the two CH_2 stretching modes are assigned around 2962 and 2686 cm^{-1}. In CA, the IR and Raman bands between 2827 and 2700 cm^{-1} are attributed to those vibration modes.

1800–1000 cm^{-1} region. This region is prone to deformation, wagging and rocking modes corresponding to NH_2, CH_2 and C–H groups [24–26,48]. Hence, the NH_2 deformation modes in FB, CA and HCl are predicted between 1640 and 1610 cm^{-1} and, hence, they are assigned to the strong IR bands at 1665 and 1650 cm^{-1}. In CA, the C6═C8 stretching mode is predicted at higher wavenumbers than the NH_2 deformation mode while in form III of HCl that deformation mode is observed together with the rocking mode of N1–H30 bond. The C═C stretching modes with double bond character are predicted in all species between 1615 and 1506 cm^{-1} while those that present partial double bond character are predicted between 1475 and 1367 cm^{-1}. Then, all those modes are assigned according to the SQM calculations, as observed in Table 4. A very important result is observed for the stretching modes of N1–C8 bonds because in CA the N1 is linked to N1–H30 bond and, hence, that N1–C8 bond is presented as simple while in FB and in the two forms of HCl are presented double bonds (see Fig. 2). For these reasons, in these two latter species the corresponding vibration modes are predicted around 1531 and 1309 cm^{-1} while in CA that N1–C8 stretching mode is predicted to 1126 cm^{-1}. In both forms of HCl those modes are predicted coupled with other mode or as pure mode in different regions (1270 and 1224 cm^{-1}). For CH_2 groups, the corresponding deformations, wagging and rocking modes are assigned between 1453/1408, 1414/1341 and 1296/1134 cm^{-1}, respectively while the rocking modes of NH_2 groups are assigned as predicted by calculations between 1151 and 1107 cm^{-1}. In this region, the other N1–C11 and N2–C9 stretching modes are also assigned for the three species because the SQM calculations predict these modes for FB and CA between 1270 and 1076 cm^{-1} while for both forms of HCl the N2–C9 stretching modes are predicted to 1499/1420 cm^{-1}.

1000–10 cm^{-1} region. Here, twisting and wagging modes of CH_2 and NH_2 are expected in this region together with C–C stretching

modes and other skeletal modes, such as CH out-of-plane deformations and deformations and torsions of three rings. In FB, the NH_2 wagging and twisting modes are predicted to 542 and 348/264 cm^{-1}, in CA appear at 730 and 205 cm^{-1}, respectively while these vibration modes in the form I of HCl are predicted to 366 and 299 cm^{-1} and in its form III to 54 and 16 cm^{-1}, respectively. Evidently, in the form III, the N2–H26 bond of NH_2 is linked to Cl31 and, for this reason, the NH_2 wagging and twisting modes in this form of HCl are predicted at lower wavenumbers than the other form. Another important remark is observed in the HCl species because in the form I the deformation modes of N1–H30–Cl31 angle is predicted to 1077 cm^{-1} while in the form III the corresponding mode δN2-H26-Cl31 is predicted to 71 cm^{-1}. Same reasons mentioned above justify such observations. The remains vibrational modes are assigned as predicted by SQM calculations (see Table 4).

4. Force constants

Here, the SQMFF approach with the Molvib program have allowed the determination of harmonic scaled force constants using the harmonic force fields of the three species of tacrine in gas phase calculated using the B3LYP/6-311G* method [41–43]. Table 5 shows the scaled internal force constants for FB, form I CA and forms I and II HCl species in gas phase compared with the reported for the antiviral rimantadine and amantadine in gas phase using the B3LYP/6–311++G** method [26,48]. If first we analyse the scaled internal force constants for FB, it is observed a higher value of *f(νN-H)* force constant associated to NH_2 group, as expected because in this species that group is free while in CA, the N1 atom is protonated instead N2 of NH_2 group and, as the protonation takes places in N1 of A2 ring that force constant is also influenced by the charge on N1. In both HCl species, the value of *f(νN-H)* force constants are lower than FB due to the presence of Cl in the bonds: N1–H30···Cl31 in form I and N2–H26···Cl31 in form III. Analysing the *f(νC-N)* force constants, the lower value is observed for CA because the charge on N1 produces enlargement of N1–C8 and N1–C11 bonds and, as a consequence decreases the values of the corresponding force constants. For the same reason, lower values are observed for this species in the *f(νC-H)* and $f(\nu C\text{-}C)_{A1}$ force constants. The differences in the values of $f(\nu C\text{-}C)_{A1}$ force constants indicate that the A1 ring is also affected by the positive charge of CA. Besides, the presence of Cl atoms in form I and III of HCl also influences the values of force constants. When the force constants of tacrine are compared with the corresponding to rimantadine and amantadine the values are different because these species present fused rings, as observed in Fig. S10 and, in CA the NH_2 is protonated as NH_3^+ while in HCl the Cl atom is linked to that charged group. Note that the $f(\nu CH_2)$ and $f(\delta CH_2)$ force constants present comparable values in the three species.

5. NMR study

Comparisons of predicted ^1H and ^{13}C NMR chemical shifts of FB, form I CA, forms I and III HCl of tacrine by using the GIAO and hybrid B3LYP/6-311G* methods with the corresponding experimental for tacrine in D_2O taken from Ref. [46] are summarized in Tables 6 and 7. The correlations between experimental and theoretical chemical shifts are expressed by RMSD values. Table 6 shows that the better concordances for the ^1H nucleus are observed between 0.2 and 1.1 ppm while for the ^{13}C nucleus the rmsd differences increase from 19 to 1.8 ppm. Thus, for the ^1H nucleus the low rmsd values are observed for FB, form I CA and form III HCl while for the form I of HCl the value increases to 1.3 ppm. In relation to the ^{13}C nucleus, both forms of HCl show better correlations than the other

Table 5
Scaled internal force constants for the free base, form I cationic and forms I and II hydrochloride species of tacrine in gas phase by using the B3LYP/6-311G* method compared with the corresponding to antiviral rimantadine and amantadine.

Force constants	B3LYP/6-311G* method					
	Tacrine[a]					
	Free base	Cationic	Form I Hydrochloride		Form III Hydrochloride	
f(νN-H)	7.36	5.91	6.91		5.34	
f(νC-N)	7.31	4.78	7.01		7.11	
f(νC-H)	5.54	4.94	5.11		5.12	
$f(\nu C\text{-}C)_{A1}$	6.75	6.05	6.33		6.38	
$f(\nu CH_2)$	5.07	4.44	4.69		4.72	
$f(\delta CH_2)$	0.79	0.73	0.72		0.72	
B3LYP/6–311++G** method						
Force constants	Rimantadine[b]			Adamantadine[c]		
	Free base	Cationic	Hydrochloride	Free base	Cationic	Hydrochloride
f(νN-H)	6.42	6.12	4.81	6.31	6.08	4.99
f(νC-N)	4.32	2.81	3.81	4.38	2.54	4.78
f(νC-H)	4.53	4.72	4.66	4.63	4.75	4.70
$f(\nu C\text{-}C)_R$	4.39	4.39	439	4.50	4.50	6.11
$f(\nu CH_2)$	4.64	4.65	4.65	4.64	4.69	4.71
$f(\delta CH_2)$	0.71	0.71	0.73	0.71	0.71	0.73

Units are mdyn $Å^{-1}$ for stretching and mdyn Å rad^{-2} for angle deformations.
[a] This work.
[b] From Ref. [26].
[c] From Ref. [48].

Table 6
Observed and calculated ^{1}H chemical shifts (δ in ppm) for the three species of tacrine in aqueous solutions by using the 6-311G* method.

H atom	B3LYP/6–311++G** Method[a]				Exp[b]
	Free base	Form I Cation	Form I Hydrochloride	Form III Hydrochloride	
16-H	1.85	1.94	1.91	1.91	1.8
17-H	1.57	1.65	1.59	1.56	1.6
18-H	2.23	2.23	2.21	2.23	2.4
19-H	2.29	2.23	2.19	2.43	2.4
20-H	1.74	1.82	1.79	1.79	1.8
21-H	1.54	1.61	1.54	1.60	1.6
22-H	2.70	2.78	2.66	2.73	2.4
23-H	2.66	2.58	2.94	2.51	2.4
24-H	7.50	7.69	7.63	7.64	7.5
25-H	7.46	7.37	7.96	7.30	7.3
26-H	3.53	5.06	4.86	7.35	7.4
27-H	3.99	5.61	5.39	5.45	4.8
28-H	7.19	7.52	7.48	7.46	7.5
29-H	7.41	7.75	7.63	7.68	7.5
30-H		8.14	11.82	7.97	7.5
RMSD[a]	**1.1**	**0.7**	**1.3**	**0.2**	

[a] This work GIAO/B3LYP/6-311G* Ref. to TMS.
[b] From Ref [45].

Table 7
Observed and calculated^{13}C chemical shifts (δ in ppm) for the three species of tacrine in aqueous solutions by using the 6-311G* method.

H atom	B3LYP/6–311* Method[a]				Exp[b]
	Free base	Form I Cation	Form I Hydrochloride	Form III Hydrochloride	
3-C	25.2	41.2	23.4	23.7	22
4-C	25.2	40.7	23.5	25.7	24
5-C	25.3	40.5	22.9	23.1	22
6-C	113.8	131.1	112.5	114.2	112
7-C	37.0	48.7	30.3	31.1	30
8-C	163.9	174.6	157.7	156.1	154
9-C	152.9	174.9	156.6	157.8	158
10-C	120.3	135.2	117.4	117.9	115
11-C	151.0	158.0	141.7	140.6	138
12-C	123.2	142.8	124.7	125.3	124
13-C	132.3	139.8	122.4	121.8	120
14-C	126.2	147.8	129.4	129.7	128
15-C	131.6	155.7	136.9	137.7	138
RMSD[a]	**6.7**	**19.0**	**1.9**	**1.8**	

[a] This work GIAO/B3LYP/6-311G* Ref. to TMS.
[b] From Ref [45].

ones. Calculations at the same level of theory for the form II of HCl show rmsd values for ^{1}H and ^{13}C NMR chemical shifts of 1.1 and 10.6 ppm, respectively suggesting that all these species of tacrine could be present in solution. Thus, the FB, CA and both forms of HCl could be present in solution although probably the high rmsd value observed in Table 7 for the form I of CA is related to used solvent and to the theoretical calculations performed with the B3LYP/6-311G* method.

6. Ultraviolet–visible spectra

The experimental electronic spectrum of tacrine hydrochloride monohydrate in methanol solution between 200 and 350 nm taken from Ref. [46] is compared in Fig. 7 with the predicted for FB and CA in aqueous solution [27]. The corresponding for the three forms of HCl compared with the experimental one are shown in Fig. S11. The experimental spectrum shows four bands with different intensities where the most intense is located at 239 nm and the less intense is placed at 216, 322 and 335 nm. In FB, a band of medium intensity, intense, very intense and weak appear at 169, 207, 234 and 307 nm, respectively while, in the spectrum of CA, the weak band is located at 229 nm, the most intense at 235 nm and the shoulder and the weak band appear at 275 and 305 nm, respectively. The absorption bands observed in FB are associated to the $\pi\rightarrow\pi^*$ and $n\rightarrow\pi^*$ transitions predicted for FB and CA species by NBO analyses. Fig. S11 shows the electronic spectra for the three forms of HCl, where form I presents two bands, a very intense at 350 nm and other weak at 450 nm. The spectrum of form II shows, between 150 and 200 nm two bands and a shoulder at 169, 170 and 175 nm and, between 200 and 350 nm three bands at 200, 225 and 290 nm, respectively. The form III of HCl shows only two bands between 400 and 700 nm, located at 475 and 650 nm. These bands are attributed to $\pi\rightarrow\pi^*$ and $\pi^*\rightarrow\pi^*$ transitions predicted by NBO analyses. These studies show the form III of HCl is not present in an electronic spectrum of tacrine in aqueous solution. However, the FB, CA and Form I

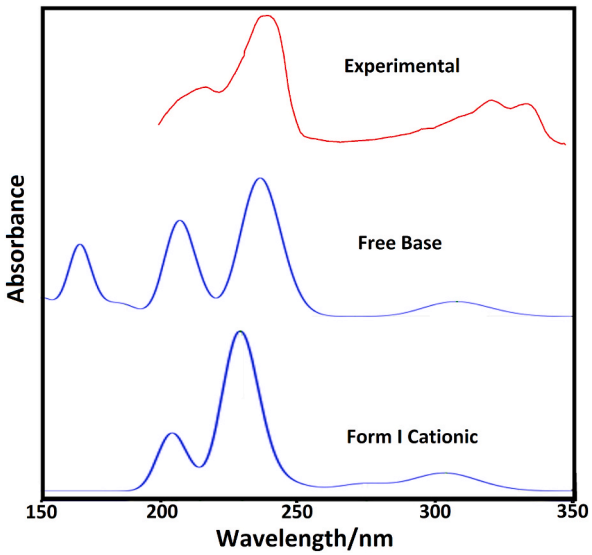

Fig. 7. Experimental electronic spectrum of tacrine hydrochloride monohydrate in methanol solution taken from Ref. [45] compared with those predicted for the freebase and form I cationic in aqueous solution by using the B3LYP/6-311G* method.

and II of HCl could be present in solution.

7. Conclusions

In this research, structures and vibrational spectra of FB, forms I and II CA and three forms of HCl, named I, II and III of cholinesterase inhibitor anhydrous tacrine were theoretically studied combining the hybrid functional B3LYP method with different basis sets (6–311++G**, 6-311G* and 6-31G*) and the SQMFF approach. The NMR, infrared and Raman spectra suggest that all these species of tacrine could be present in solution while the predicted electronic spectra for all forms evidence that the form III of HCl is not present in an electronic spectrum of tacrine in aqueous solution probably due to the fact that this species is as cationic one. The energy values show that the three forms of HCl can exist in both media because the energy decreases from 35.15 kJ/mol in gas phase to 5.51 kJ/mol in solution. The stability order observed for the most stable species of tacrine by NBO analyses is the following: form I HCl > form III HCl > form I CA > FB. CA species presents the highest solvation energy value, as reported for different alkaloids and antihypertensive agents. The structure of form III of HCl present better concordance and lower RMSDs because this form corresponds to that experimental observed in solid phase. The higher topological properties of form III in the two media could justify experimentally its presence in the both media. The strong N2–H26···Cl31 interaction justifies the higher stability of form III in both media. Evaluation of gap values support the higher reactivity of form III while FB is the less reactive species in both media. Complete assignments of 81, 84 and 87 vibration modes expected for FB, CA and HCl species are reported together with the corresponding scaled force constants using the B3LYP/6-311G* method and the SQMFF methodology.

Author contribution statement

Tom Sundius: Performed experiments and calculations, analysed and interpreted the data.

Silvia Antonia Brandán: Conceived and designed the experiments; contributed reagents, materials, analysed and interpreted the data; Wrote the paper.

Funding statement

This research did not receive any specific grant from funding agencies in the public, commercial, or not-for-profit sectors.

Data availability statement

Data will be made available on request.

Declaration of competing interest

The authors declare the following financial interests/personal relationships which may be considered as potential competing interests:The authors declare the following conflict of interests: Silvia Antonia Brandán is part of the Editorial Board for Heliyon

Chemistry.

Acknowledgements

This work was supported by Consejo de Investigaciones Universidad Nacional de Tucumán (CIUNT) Project No. 26/D714.

Appendix A. Supplementary data

Supplementary data to this article can be found online at https://doi.org/10.1016/j.heliyon.2023.e17280.

References

[1] K.L. Davis, L.J. Thal, E.R. Gamzu, et al., A double blind, placebo-controlled multicenter study of tacrine for Alzheimer's disease. The Tacrine Collaborative Study Group, N. Engl. J. Med. 327 (18) (1992), https://doi.org/10.1056/nejm199210293271801. ISSN 0028-4793.
[2] A.J. Wagstaff, D. McTavish, Review of its pharmacodynamic and pharmacokinetic properties, and therapeutic efficacy in Alzheimer's disease, Drugs Aging 4 (1994) 510–540.
[3] R.C. Gupta, Encyclopedia of Toxicology, third ed., Tacrine, 2014, pp. 466–467, https://doi.org/10.1016/B978-0-12-386454-3.00198-6.
[4] M. Girek, P. Szymański, Phyto-tacrine hybrids as promising drugs to treat Alzheimer's disease, medicinal Chemistry & drug discovery, ChemistrySelect 4 (2019) 5776–5790, https://doi.org/10.1002/slct.201803672.
[5] I. Vieira, L.T.F.M. Camargo, L. Ribeiro, A.C.C. Rodrigues, A.J. Camargo, Structure-activity relationship of tacrine and its analogues in relation to inhibitory activity against Alzheimer's disease, J. Mol. Model. 25 (2019) 116, https://doi.org/10.1007/s00894-019-3993-8.
[6] C. Remya, K.V. Dileep, E.K. Reddy, K. Mantosh, K. Lakshmi, R.S. Jacob, A.M. Sajith, E.J. Variyar, S. Anwar, K.Y.J. Zhang, C. Sadasivan, R.V. Omkumar, Neuroprotective derivatives of tacrine that target NMDA receptor and acetyl cholinesterase-Design, synthesis and biological evaluation, Comput. Struct. Biotechnol. J.. https://doi.org/10.1016/j.csbj.2021.07.041.
[7] M.V. Grishchenko, G.F. Makhaeva, Y.V. Burgart, E.V. Rudakova, N.P. Boltneva, N.V. Kovaleva, O.G. Serebryakova, S.V. Lushchekina, T.Y. Astakhova, E. F. Zhilina, E.V. Shchegolkov, R.J. Richardson, V.I. Saloutin, Conjugates of tacrine with salicylamide as promising multitarget agents for Alzheimer's disease, ChemMedChem (1–6) (2022), e202200080, https://doi.org/10.1002/cmdc.202200080.
[8] M. Alam, D.- U Lee, Synthesis, spectroscopic and computational studies of 2-(thiophen-2- yl)-2,3-dihydro-1H-perimidine: an enzymes inhibition study, Comput. Biol. Chem. 64 (2016) 185–201.
[9] M. Przybyłowska, S. Kowalski, K. Dzierzbicka, I. Inkielewicz-Stepniak, Therapeutic potential of multifunctional tacrine analogues, Curr. Neuropharmacol. 17 (2019) 472–490, https://doi.org/10.2174/1570159X16666180412091908.
[10] R. Rajeshwari, K. Chand, E. Candeias, S.M. Cardoso, S. Chaves, M.A. Santos, New multitarget hybrids bearing tacrine and phenylbenzothiazole motifs as potential drug candidates for Alzheimer's disease, Molecules 24 (2019) 587, https://doi.org/10.3390/molecules24030587.
[11] N. Acar Selçuki, The amidine formed by tacrine and saccharin revisited: an ab initio investigation of structural, electronic and spectroscopic properties, Turkish computational and theoretical Chemistry Turkish, Comp Theo Chem (TC&TC) 3 (1) (2019) 25–37, https://doi.org/10.33435/tcandtc.486573, e-ISSN: 2602-3237.
[12] M. Eslami, S.J. Nikkhah, S.M. Hashemianzadeh, S.A.S. Sajadi, The compatibility of Tacrine molecule with poly(n-butylcyanoacrylate) and Chitosan as efficient carriers for drug delivery: a molecular dynamics study, Eur. J. Pharmaceut. Sci. 82 (2016) 79–85, https://doi.org/10.1016/j.ejps.2015.11.014.
[13] B. Svobodova, E. Mezeiova, V. Hepnarova, M. Hrabinova, L. Muckova, T. Kobrlova, D. Jun, O. Soukup, M.L. Jimeno, J.M. Contelles, J. Korabecny, Exploring structure-activity relationship in tacrine-squaramide derivatives as potent cholinesterase inhibitors, Biomolecules 9 (2019) 379, https://doi.org/10.3390/biom9080379.
[14] K.Y. Wong, A.G. Mercader, L.M. Saavedra, B. Honarparvar, G. P Romanelli, P.R. Duchowicz, QSAR analysis on tacrine-related acetylcholinesterase inhibitors, J. Biomed. Sci. 21 (2014) 84.
[15] W.-Y. Wua, Y.- C Daia, N.-G. Lia, Z.-X. Donga, T. Gua, Z.-H. Shia, X. Xuea, Y.-P. Tanga, J.-A. Duana, Novel multitarget-directed tacrine derivatives as potential candidates for the treatment of Alzheimer's disease, J. Enzym. Inhib. Med. Chem. 32 (1) (2017) 572–587, https://doi.org/10.1080/14756366.2016.1210139.
[16] Z. Zhang, F. Fan, W. Luo, Y. Zhao, C. Wang, Molecular dynamics revealing a detour-forward release mechanism of tacrine: implication for the specific binding characteristics in butyrylcholinesterase, Front. Chem. 8 (2008) 730, https://doi.org/10.3389/fchem.2020.00730.
[17] M. Sorrenti, L. Catenacci, G. Bruni, B. Luppi, F. Bigucci, G. Bettinetti, Solid-state characterization of tacrine hydrochloride, J. Pharmaceut. Biomed. Anal. 63 (7) (2012) 53–61, https://doi.org/10.1016/j.jpba.2011.12.023.
[18] S. Bencharit, C.L. Morton, J.L. Hyatt, P. Kuhn, M.K. Danks, P.M. Potter, M.R. Redinbo, Crystal structure of human carboxylesterase complexed with the Alzheimer's drug tacrine: from binding promiscuity to selective inhibition, Chem. Biol. 10 (2003) 341–349, https://doi.org/10.1016/S1074-5521(03)00071-1.
[19] F. Nachon, E. Carletti, C. Ronco, M. Trovaslet, Y. Nicolet, L. Jean, P.-Y. Renard, Crystal structures of human cholinesterases in complex with huprine W and tacrine: elements of specificity for anti-Alzheimer's drugs targeting acetyl- and butyryl-cholinesterase, Biochem. J. 453 (2013) 393–399, https://doi.org/10.1042/BJ20130013.
[20] S. Hamulakova, L. Janovec, M. Hrabinova, K. Spilovska, J. Korabecny, P. Kristian, K. Kuca, J. Imrich, Synthesis and biological evaluation of novel tacrine derivatives and tacrine-coumarin hybrids as cholinesterase inhibitors, J. Med. Chem. 57 (2014) 7073–7084, https://doi.org/10.1021/jm5008648.
[21] Z. Najafi, M. Mahdavi, M. Saeedi, E. Karimpour-Razkenari, N. Edraki, M. Sharifzadeh, M. Khanavi, T. Akbarzadeh, Novel tacrine-coumarin hybrids linked to 1,2,3-triazole as anti-Alzheimer's compounds: ***in vitro*** and ***in vivo*** biological evaluation and docking study, Bioorg. Chem. 83 (2019) 303–316, https://doi.org/10.1016/j.bioorg.2018.10.056.
[22] S. Okten, M. Ekiz, Ü.M. Koçyigit, A. Tutar, I. Çelik, M. Akkurt, F. Gokalp, P. Taslimi, I. Gülçin, Synthesis, characterization, crystal structures, theoretical calculations and biological evaluations of novel substituted tacrine derivatives as cholinesterase and carbonic anhydrase enzymes inhibitors, J. Mol. Struct. 1175 (2019), 906e915, https://doi.org/10.1016/j.molstruc.2018.08.063.
[23] M. Moris, T. De Samber, J. Vrijdag, W. De Borggraeve, L. Van Meervelt, Crystal structure of the orthorhombic pseudopolymorph for tacrine hydrochloride, Jeroen Jacobs, Acta Crystallogr. B72 (2016) 771–774, https://doi.org/10.1107/S2052520616011094.
[24] R.A. Rudyk, M.A. Checa, C.A.N. Catalán, S.A. Brandán, Structural, FT-IR, FT-Raman and ECD studies on the FB, CA and hydrobromide species of scopolamine alkaloid, J. Mol. Struct. 1180 (2019) 603–617, https://doi.org/10.1016/j.molstruc.2018.12.040.
[25] M.E. Manzur, S.A. Brandán, S(-) and R(+) species derived from Antihistaminic promethazine agent: structural and vibrational studies, Heliyon 5 (2019), e02322, https://doi.org/10.1016/j.heliyon.2019.e02322.
[26] M.A. Iramain, J. Ruiz Hidalgo, T. Sundius, S.A. Brandán, A combined study on structures and vibrational spectra of antiviral rimantadine using SQMFF and DFT calculations, Heliyon 8 (2022), e10102, https://doi.org/10.1016/j.heliyon.2022.e10102.
[27] M.J. Frisch et al, Gaussian, Inc., Wallingford CT, 2009.
[28] A.D. Becke, Density-functional exchange-energy approximation with correct asymptotic behavior, Phys. Rev. A38 (1988) 3098–3100.

[29] C. Lee, W. Yang, R.G. Parr, Development of the Colle-Salvetti correlation-energy formula into a functional of the electron density, Phys. Rev. B37 (1988) 785–789.
[30] M.V. Castillo, M.A. Iramain, L. Davies, M.E. Manzur, S.A. Brandán, Evaluation of the structural properties of powerful pesticide dieldrin in different media and their complete vibrational assignment, J. Mol. Struct. 1154 (2018) 392–405, https://doi.org/10.1016/j.molstruc.2017.10.065.
[31] A.B. Nielsen, A.J. Holder, Gauss View 5.0, User's Reference, GAUSSIAN Inc., Pittsburgh, PA, 2008.
[32] S. Miertus, E. Scrocco, J. Tomasi, Electrostatic interaction of a solute with a continuum, Chem. Phys. 55 (1981) 117–129.
[33] J. Tomasi, J. Persico, Molecular interactions in solution: an overview of methods based on continous distributions of the solvent, Chem. Rev. 94 (1994) 2027–2094.
[34] A.V. Marenich, C.J. Cramer, D.G. Truhlar, Universal solvation model based on solute electron density and a continuum model of the solvent defined by the bulk dielectric constant and atomic surface tensions, J. Phys. Chem. B113 (2009) 6378–6396.
[35] P. Ugliengo, MOLDRAW Program, University of Torino, Dipartimento Chimica IFM, Torino, Italy, 1998.
[36] E.D. Glendening, J.K. Badenhoop, A.D. Reed, J.E. Carpenter, F. Weinhold, NBO 3.1; Theoretical Chemistry Institute, University of Wisconsin, Madison, WI, 1996.
[37] R.F.W. Bader, Atoms in Molecules, A Quantum Theory, Oxford University Press, Oxford, 1990, 0198558651.
[38] F. Biegler-Köning, J. Schönbohm, D. Bayles, AIM 2000; A program to Analyze and visualize atoms in molecules, J. Comput. Chem. 22 (2001) 545.
[39] B.H. Besler, K.M. Merz Jr., P.A. Kollman, Atomic charges derived from semiempirical methods, J. Comput. Chem. 11 (1990) 431–439.
[40] R.G. Pearson, Absolute electronegativity and hardness correlated with molecular orbital theory, Proc. Natl. Acad. Sci. U.S.A. 83 (1986) 8440–8441.
[41] R.G. Parr, L.V. Szentpaly, S. Liu, Electrophilicity index, J. Am. Chem. Soc. 121 (1999) 1922–1924.
[42] P. Pulay, G. Fogarasi, G. Pongor, J.E. Boggs, A. Vargha, Combination of theoretical ab initio and experimental information to obtain reliable harmonic force constants. Scaled quantum mechanical (QM) force fields for glyoxal, acrolein, butadiene, formaldehyde, and ethylene, J. Am. Chem. Soc. 105 (1983) 7073, https://doi.org/10.1021/ja00362a005.
[43] G. Rauhut, P. Pulay, Transferable scaling factors for density functional derived vibrational force fields, J. Phys. Chem. 99 (1995) 3093–3100, https://doi.org/10.1021/j100010a019.
[44] T. Sundius, Scaling of ab-initio force fields by MOLVIB, Vib. Spectrosc. 29 (2002) 89–95.
[45] Available from Web page.https://spectrabase.com/spectrum.
[46] G. Keresztury, S. Holly, G. Besenyei, J. Varga, A.Y. Wang, J.R. Durig, Vibrational spectra of monothiocarbamates-II. IR and Raman spectra, vibrational assignment, conformational analysis and ab initio calculations of S-methyl-N,N-dimethylthiocarbamate, Spectrochim. Acta 49A (1993) 2007–2026.
[47] R. Ditchfield, Self-consistent perturbation theory of diamagnetism. I. A gage-invariant LCAO (linear combination of atomic orbitals) method for NMR chemical shifts, Mol. Phys. 27 (1974) 714–722.
[48] S.A. Brandán, Normal internal coordinates Force fields and vibrational study of species derived from antiviral adamantadine, Int. J. Quant. Chem. 121 (2) (2021), e26425, https://doi.org/10.1002/qua.26425.